J. Min. Metall. Sect. B-Metall. 51 (1) B (2015) 7 - 15

Journal of Mining and Metallurgy, Section B: Metallurgy

COMPUTATIONAL MODELING OF ANODIC CURRENT DISTRIBUTION AND ANODE SHAPE CHANGE IN ALUMINIUM REDUCTION CELLS

Y. Xu, J. Li *, H. Zhang, Y. Lai

School of Metallurgy and Environment, Central South University, Changsha, Hunan, China

(Received 23 February 2014; accepted 17 December 2014)

Abstract

In aluminium reduction cells, the profile of a new carbon anode changes with time before reaching a steady state shape, since the anode consumption rate, depending on the current density normal to anode surfaces, varies from one region to another. In this paper, a two-dimension model based on Laplace equation and Tafel equation was built up to calculate the secondary current distribution, and the shift of anode shape with time was simulated with arbitrary Lagrangian-Eulerian method. The time it takes to reach the steady shape for the anode increases with the enlargement of the width of the channels between the anodes or between the anode and the sidewall. This time can be shortened by making a sloped bottom or cutting off the lower corners of the new anode. Forming two slots in the bottom surface increases the anodic current density at the underside of the anode, but leads to the enlargement of the current at the side of the anode.

Keywords: aluminium reduction cell, secondary current distribution, anode consumption, anode shape

1. Introduction

Aluminum is produced using Hall–Héroult process by reducing alumina in aluminium reduction cells, the schematic geometry of which is illustrated in fig. 1. In the production, the intense electrolysis current flows downwards from prebaked carbon anodes at top, passing through a molten electrolyte (bath) layer and a liquid aluminium (metal) pad before being collected at the cathode lining at bottom. Aluminium is deposited on the bath-metal interface and CO_2 is evolved from anode surfaces. The primary reaction in this process is $2Al_2O_3+3C=4Al+3CO_2$

The anode surfaces adjacent to the electrolyte include the horizontal underside surfaces and the vertical side surfaces. Most current passes through the underside of anodes, which are normally defined as working face, while, some current also passed through the vertical sides. The current distribution on the anode surfaces, especially the fraction of side current, has important influence on the cell voltage and current efficiency [1], which are the two key technical parameters for the industrial production. In addition, the carbon anode is consumed by the anodic reaction. After a new cold anode is inserted into the cell, its lower surface is immediately covered by the insulated frozen electrolyte, which slowly melts away in the first 12~18 hours [2]. When the anode surface is exposed to the molten electrolyte, the anodic reaction takes place and the shape of the anode begins to transform. The shift of anode shape causes the variation of the electromagnetic fields in the cell, which can lead to instability of the working condition of the cell. Consequently, the anodic current distribution and the shift of the anode shape with respect to time need to be analyzed precisely.

The current distribution in aluminium reduction cells has been widely studied. Different approaches have been adopted to study the two approximations of anodic current distribution, primary current distribution [1, 3-5] and secondary current distribution [6-8]. The former defines the anodic overvoltage as a constant value, but the latter introduces the overvoltage depending on the local current density. In reference [9, 10], the second current distribution for a 150 kA prebaked cell was studied, and the shift of the anode shape was calculated with the methods of incremental time steps and "near steady state shape" condition. The study showed it normally took 6 to 8 days until a steady shape anode was obtained, depending on the width of the channels between the two anodes or between the anode and the sidewall. In reference [11], a similar study for the anode with chamfers was carried out, and the results indicated it took less time to reach the steady shape for the anode whose lower corner were cut off by 5 cm (diagonally), as compared to the anode with rectangular corners. In these studies, the current density at the underside of the anode was assumed as a constant value (0.75 $A \cdot cm^{-2}$), and it was ignored that the local current density at the underside varied with distance from the edge, which could result in an

* *Corresponding author: sqjsxu@gmail.com*

DOI:10.2298/JMMB140223006X

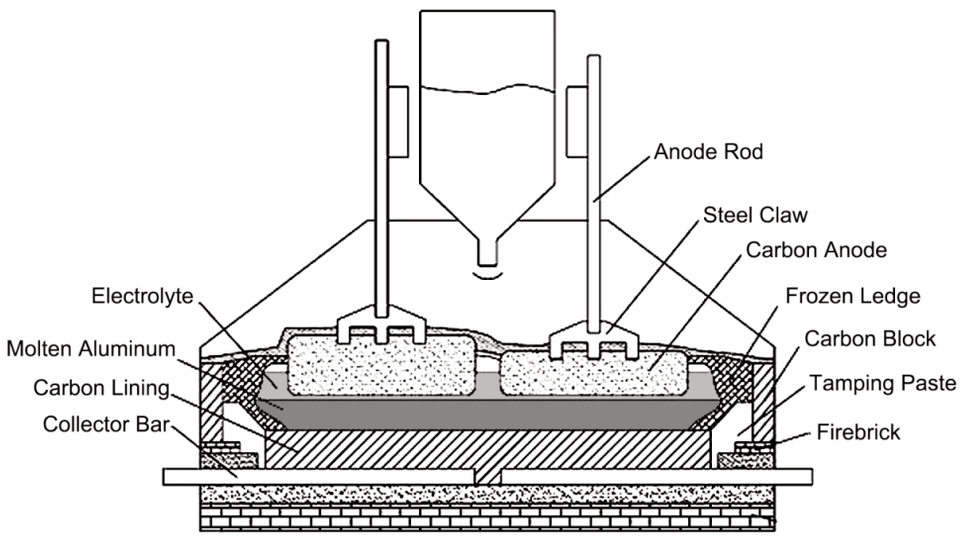

Figure 1. *Schematic geometry of a modern aluminum reduction cell*

inaccuracy that the current density varies smoothly near the corner.

In this paper, a transient calculation for the secondary current distribution and the change of anode shape was carried out with a new model, and the Arbitrary Lagrangian-Eulerian (ALE) based finite element method was used in solving this moving-boundary problem. In addition to the normal anode with rectangular corners, the anodes with specific initial shape, including a sloped bottom, chamfers and slots, which are widely adopted in aluminium electrolysis industry, were taken into account, and the processes of shape transformations for the different anodes have been revealed.

2. Theory

2.1 Assumption

To simplify the computational model, some assumptions were made firstly. The current distribution on the anode is significantly affected by the width of the adjacent channel where the bath conducts a small part of the current from the anode. The channels and their typical widths are shown in Fig.2. Because the sidewall of the cell is always covered by a ledge of frozen bath, the real widths of the side and end channels are about 12~18 cm. In this work, a 15 cm wide channel and a 2 cm wide channel were chosen to represent the side channel and half the inter-anode channel, respectively. Considering the symmetry of electric field, it is feasible to use half the width of the inter-anode channel when modelling a single anode at one side of the inter-anode channel. The real shape of the ledge was not taken into account.

The new cold anode is covered with the ledge that melts slowly, and the different parts of anode surface are not exposed to the bath at the same time. There is small current passing through some parts of the surfaces during the heating-up period, which was ignored in this work. The initial time for the calculation was taken as the time when the entire anode is clear of the ledge. The gas bubbles generated by the anodic reaction usually form a thin gas film underneath the anode, while, the resistance of the gas film was not taken into account in the calculation. The influence of the wave of the bath-metal interface was also neglected.

The electrical conductivities of liquid aluminum, typical carbon anode and molten electrolyte are 3.5×10^{6} $s\cdot m^{-1}$ [12], 2.1×10^{4} $s\cdot m^{-1}$ [13] and 2.2×10^{2} $s\cdot m^{-1}$ [12], respectively. According to the huge disparity of the three conductivities, it can be assumed that the anode surface and the bath-metal interface are approximately equipotential surfaces [9, 14].

When the corners of the anode become round owing to the consumption, the explicit line dividing the side surface and bottom surface disappears. To be

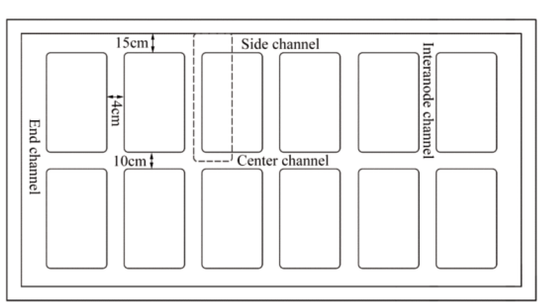

Figure 2. *The channels and their typical widths in the aluminium reduction cell*

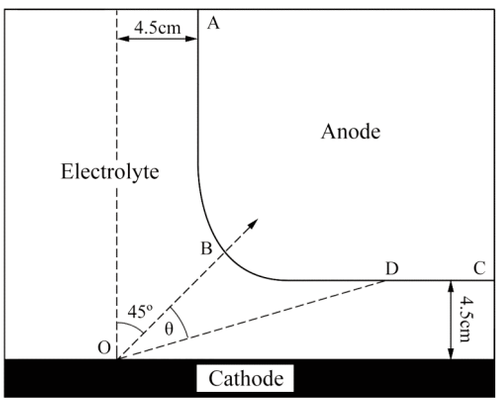

Figure 3. *Schematic cross section of a prebaked anode in the aluminium reduction cell*

convenient for presenting the results, the anode surface was artificially divided as shown in fig. 3. The anode-cathode distance (so-called ACD) was taken to be 4.5 cm in this work. The part of the anode curve going from point A, the surface of the bath, to point B was defined as the side of the anode, and the rest part of the curve going from point B to point C was regarded as the underside of the anode. Obviously, there is a one-to-one correspondence between the arbitrary point D on the anode curve and the angle θ made by the line OB and OD. The positive angle θ corresponds to the underside of the anode, while, the negative angle θ corresponds to the side of the anode.

2.2 Computational model

The distribution of the electric potential ϕ in the interelectrode space can be described by the Laplace equation:

$$\nabla^2\phi = 0 \tag{1}$$

The current density, J, at any point was determined from the gradient of local potential, ϕ, according to Ohm's Law:

$$J = -\sigma\nabla\phi \tag{2}$$

Where σ is the electric conductivity of the molten electrolyte.

The model for the second current distribution can be established by characterizing the boundary conditions. The potential at the anode surface was defined to be zero, so the inner potential of the electrolyte at the anode surface ϕ_a can be given by Tafel equation:

$$-n\cdot J = J_0\cdot\exp(-\frac{\phi_a}{b_c}) \tag{3}$$

Where the current density J is in A·m^{-2}, the potential ϕ_a is in V, n denotes the unit vector normal to the anode surface, and J_0=100 A·m^{-2}, b_c=0.109 V [9]. In this work, the current density at the underside of the anode was not assumed to be a constant value, and the magnitude of the current entering into the system was controlled by the equation that described the inner potential of the electrolyte at the metal-bath interface ϕ_m:

$$-\int\sigma\cdot\frac{\partial\phi_m}{\partial n} = I \tag{4}$$

Where I is the total current flowing across the metal-bath interface, and the value of I was determined by the average current density at the underside of the anode, which was chosen to be 0.78 A·cm^{-2} in this work. The other boundaries for the electric field were defined to be insulated.

When the anode is consumed, the boundaries of the model move. The moving velocity of the anode surface is equal to the anode consumption rate, which is proportional to the normal current density to the anode surface J_n. Defining the anode contour as $y=G(x)$, the movement of a point on the anode surface can be described as

$$\frac{ds_n(x,G(x))}{dt} = -k\cdot J_n(x,G(x)) \tag{5}$$

With

$$k = \frac{3\eta}{F\rho} \tag{6}$$

Here $s_n(x, G(x))$ is the normal moving distance of the point $(x, G(x))$, t is the time of electrolysis, k is a coefficient for describing the relationship between normal current density and movement velocity for a point on anode surface, F is Faraday constant, ρ is the anode density, and η is a factor to describe the overconsumption of the anode with respect to the Faraday's law. It is widely recognized that the overconsumption is caused by dusting and the Boudouard reaction [15]. The anode density ρ and factor η were taken to be 1.55 g/cm^3 and 1.15, respectively, and then k is 8.251×10^{-8} m^{3}A^{-1}h^{-1}.

With the consumption of the anode, the molten aluminium is produced at the top surface of the metal and the metal-bath interface moves upward simultaneously. The metal-bath interface commonly moves up a little faster than the anode bottom surface, while, to maintain a steady cell voltage (a constant ACD), the vertical location of the anodes is adjusted frequently in industry. In this study, the velocity of the metal-bath interface was set following the principle that the average ACD didn't change with time.

This two-dimension transient model was solved with finite element method by discretizing the computational domain with quadrate elements. To track the moving boundary but avoid the reduction of the mesh quality, Arbitrary Lagrangian-Eulerian (ALE) method was adopted. In the calculation, the meshes on the boundaries move along with the boundaries, and the meshes inside the domain move arbitrarily to optimize the shapes of elements. Considering that the speed of the

anode consumption is quite slow (about 1.5 cm per day), the time step of the transient computation was taken to be 2 hours, and a sufficient number of steps were executed (more than 120 steps). The calculation started with the initial shape of an anode, and the steady state shape of the anode and the secondary current distribution were achieved after the calculation.

3. Results and discussion

3.1 The influence of the width of the channel

The distributions of the current densities and equipotential lines in the interelectrode space at different time during the electrolysis for the 15 cm channel and the 2 cm channel were shown in fig.4 and fig.5, respectively, in which the shift of anode contours also can be seen. The current density concentrates at the corner of the anode at the initial time, which makes the consumption rate at the corner larger than in other regions. In the first 1 to 2 days the rectangular corners become round, and the radian of the anode curves increases with the time going. A constant anode shape was obtained after 8 days for the 15cm channel, however, the shape of the anode reaches a steady state after 7 days for the 2 cm channel. It takes more time to arrive a constant shape for the anode adjacent to a wider channel, which agrees with the conclusions reported in reference [9].

The distributions of the anodic current densities for the two cases are presented in fig.6 and fig.7, respectively. The anode curves are divided by the line θ=0, the right of which corresponds to the undersides of the anodes. From fig.6 or fig.7, one can see that the sharp peak of the anodic current density lies at the rectangular corner (θ=0) at the initial time. The peak moves towards the right and becomes gentle with the process of the electrolysis, and it disappears when the steady shape of the anode is achieved. The transformation of the anode shape decreases the anodic current density nearby the corner, increases the anodic current densities at both the bottom and side surfaces, and makes the anodic current distribute more uniformly. As the anode changes from the initial shape to the steady-state shape, the ratio of the average current density at the underside of the anode to that at the side of the anode decreases from 2.82 to 2.55 for the 15 cm channel, while, this ratio decreases from 10.92 to 8.36 for the 2 cm channel. It is indicated that the proportion of the current passing through the side of the anode in the total current increases during the change of the anode shape and this proportion is amplified by enlarging the width of the channel.

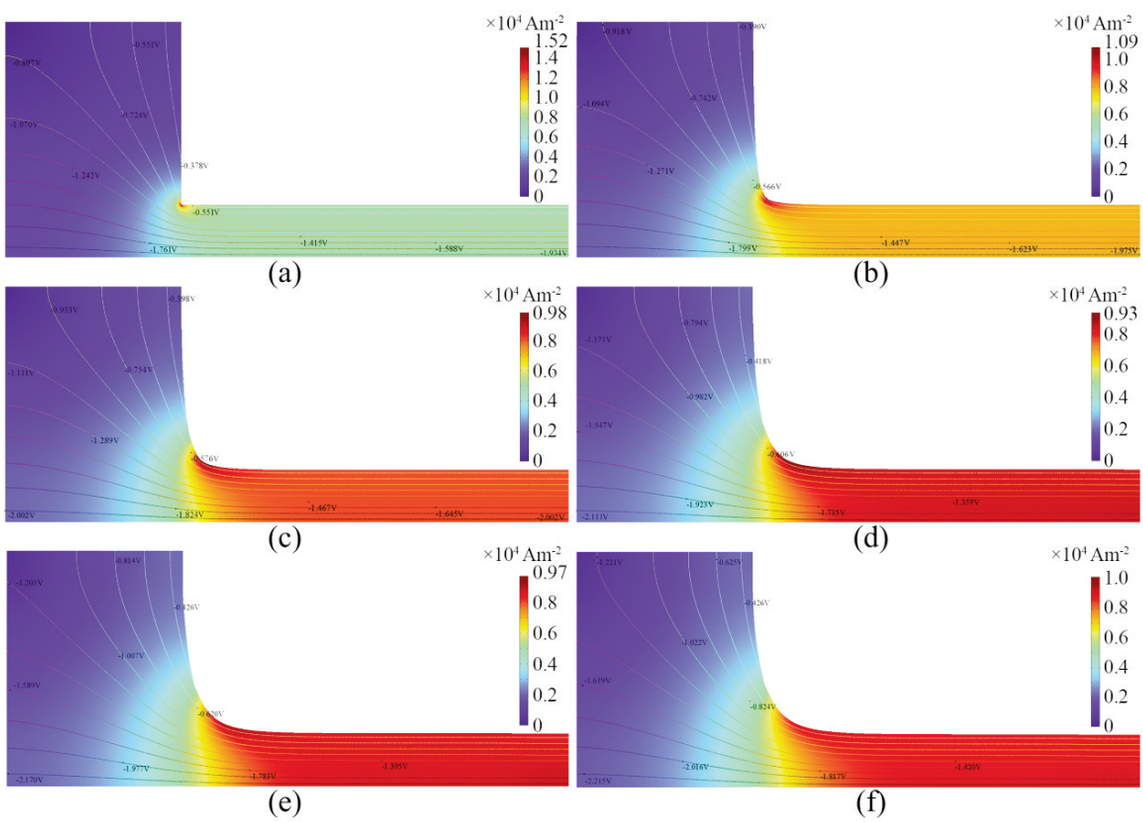

Figure 4. *The anode shapes and secondary current distributions for the 15cm channel at (a) the initial time, after (b) 1 day, (c) 2 days, (d) 4 days, (e) 6 days and (f) 8 days.*

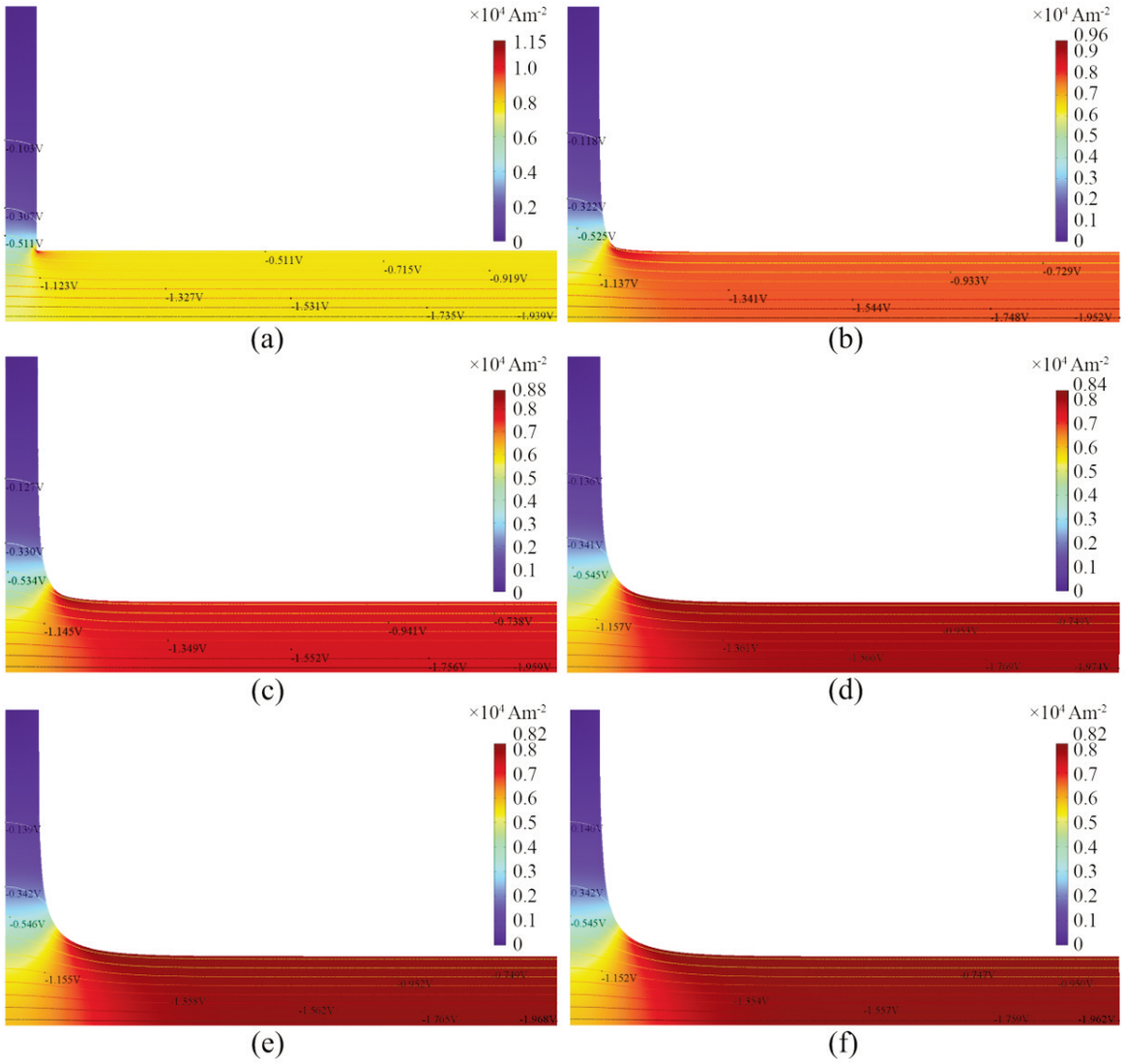

Figure 5. *The anode shapes and secondary current distributions for the 2cm channel at (a) the initial time, after (b) 1 day, (c) 2 days, (d) 4 days, (e) 6 days and (f) 7 days.*

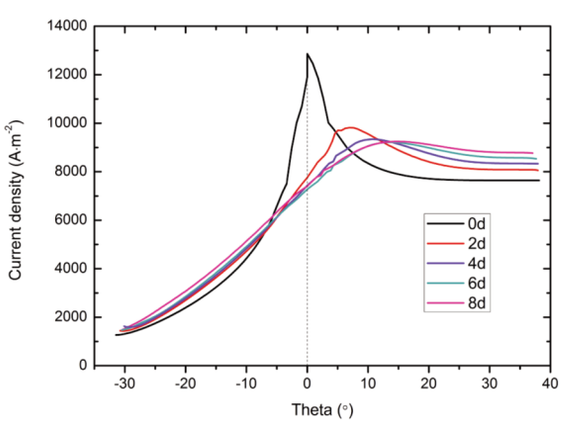

Figure 6. *The distributions of the anodic current densities at different time for the 15cm channel.*

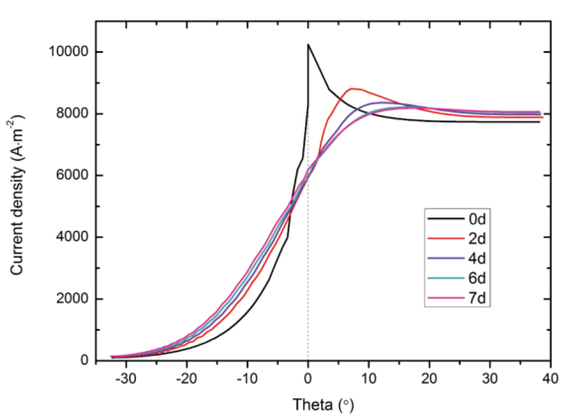

Figure 7. *The distributions of the anodic current densities at different time for the 2cm channel.*

3.2 The influence of the initial shape of anode

In order to reduce the thickness of the gas layer underneath the anode, the anodes are designed to facilitate the release of gas bubbles. The anodes with chamfers, slots or sloped bottoms are widely used in industry, and the shape transformations during the electrolysis for these specific anodes were also analyzed in this work.

The anode with chamfers is commonly produced by cutting off the corners between the bottom surface and the larger side surface of a rectangular anode. Fig. 8 shows the calculated results for the anode whose lower corners were cut off by 4 cm (diagonally). It can be found that the bevel turns into a round corner in the first two days, and the steady shape of the anode is obtained after 6 days, which is shorter than the time it takes for the normal anode. The anodic current densities for the normal anode and the anode with chamfers both reach maximums nearby the corners, and the maximums are compared in fig. 9. It can be seen from fig. 9 that the maximum anodic current density for the anode with chamfers keeps smaller than that for the normal anode from one day after the electrolysis began to the time when the same constant shapes are achieved. The maximum anodic current density for the anode with chamfers is quite larger at the initial time, but it decreases very fast in the first day.

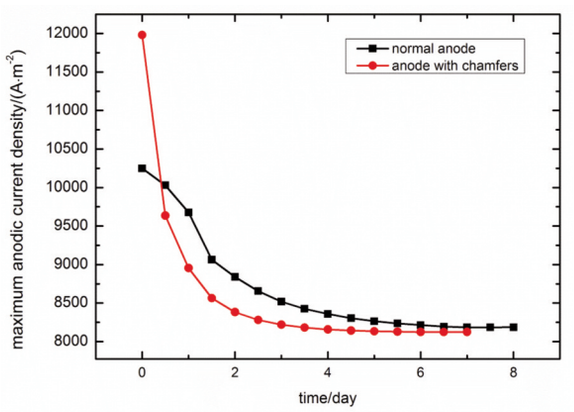

Figure 9. *The changes of the maximum anodic current densities with respect to time for the normal anode and the anode with chamfers.*

The same computation for the anode with a sloped bottom was carried out. The tilted angle of the bottom surface of the initial anode was chosen to be 1.7 degrees, and the calculated anode shapes and secondary current distributions at different time during the electrolysis are shown in fig. 10. Comparing fig. 10 with fig. 4, one can see that the sloped bottom facilitates the transformation of the anode from its initial shape to the steady shape. It takes only 5.5 days to reach the constant shape for this anode, comparative to 8 days for the normal anode. As

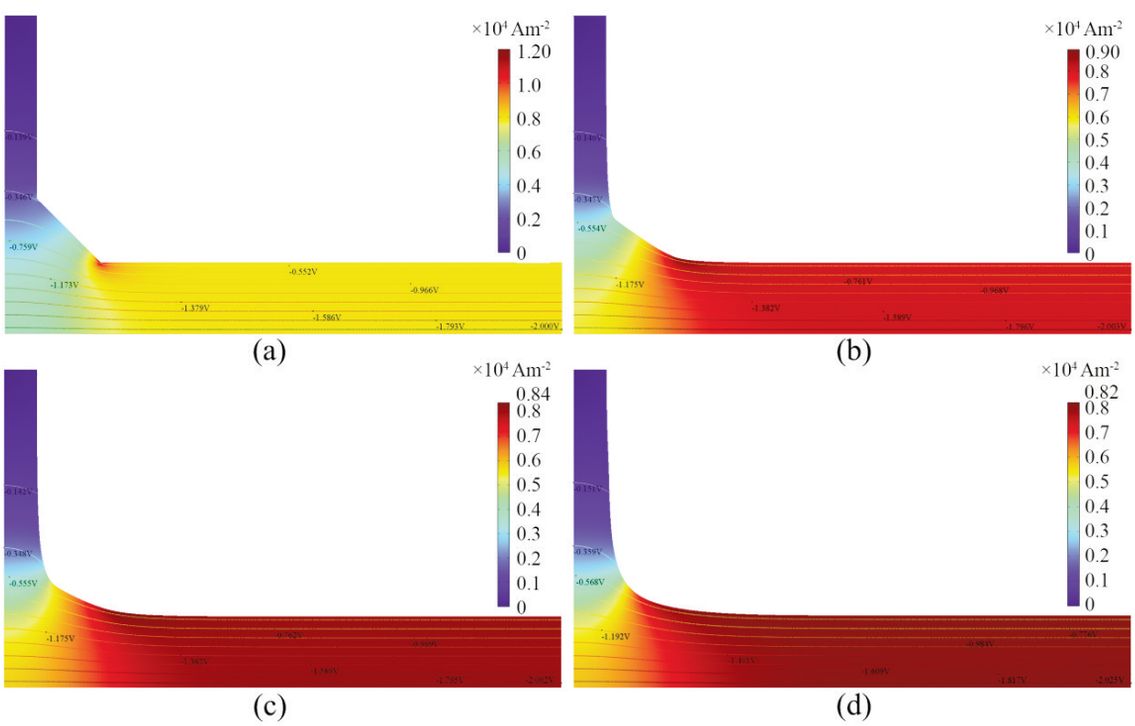

Figure 8. *The anode shapes and secondary current distributions for the anode with chamfers (cutting off the lower corners by 4cm) at (a) the initial time, after (b) 1 day, (c) 2 days and (d) 6 days.*

shown in fig. 11, the maximum anodic current density for the anode with a sloped bottom has maintained smaller than that for the normal anode until the same steady shape of the anodes is obtained, which, to some extent, indicates the tilted bottom makes the anodic current density distributes more uniformity in the early period of the electrolysis.

The anode with slots was also taken into consider in our work. It is common to form two slots in the bottom surface of the new anode. The slot is the same length as the anode, and its typical width is no more than 2 cm. The calculated secondary current distributions and profiles of half the anode with slots, whose width is taken to be 1cm, are shown in fig. 12. The rectangular corner formed by the slot also gradually turns into a round one after the electrolysis starts, and it takes 7 days for this anode to reach the steady shape. Obviously, the slot is an equivalent channel that is narrower than other channels, and the shape transformation of the corner adjacent to the slot completes faster, hence, the existence of the slot doesn't extend the time it needs to arrive the constant shape for the anode. The slot reduces the area of the working face of the anode and divides the bottom surface into two different regions, which results in the redistribution of the anodic current. The average anodic current densities in the regions of the underside of the anode with slots are compared to that at the underside of the normal anode in fig. 13, where region A indicates the bottom surface between the two slots of the anode with slots, region B indicates the bottom surface of the anode with slots except the region A, and region C indicates the entire bottom surface of the normal

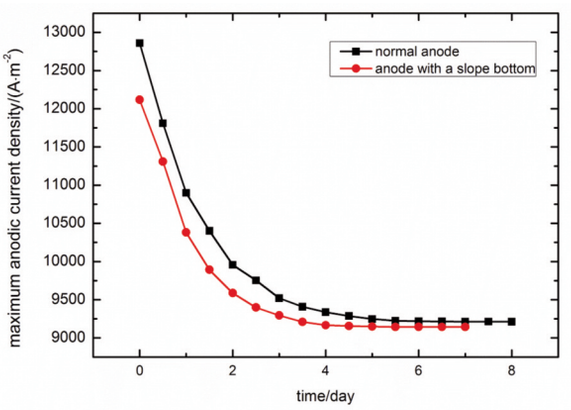

Figure 11. *The changes of the maximum anodic current densities with respect to time for the normal anode and the anode with a sloped bottom.*

anode without slots. The average anodic current density in region A is smaller than that in region B at the initial time, and the latter maintains larger than the former until the shape of the anode doesn't change any more. After the first day of the electrolysis, the average anodic current density in region A becomes larger than that in region C, which is smaller than that in region B throughout the electrolysis. It is proved that the reduction of the area of the bottom surface enlarges the anodic current density at the underside. When the steady shapes of the anodes are reached, the average anodic current densities at the side surfaces of the anode with slots and the normal anode are, respectively, 1020 $A \cdot m^{-2}$ and 960 $A \cdot m^{-2}$, which manifests the slot also enlarges the anodic current at the side.

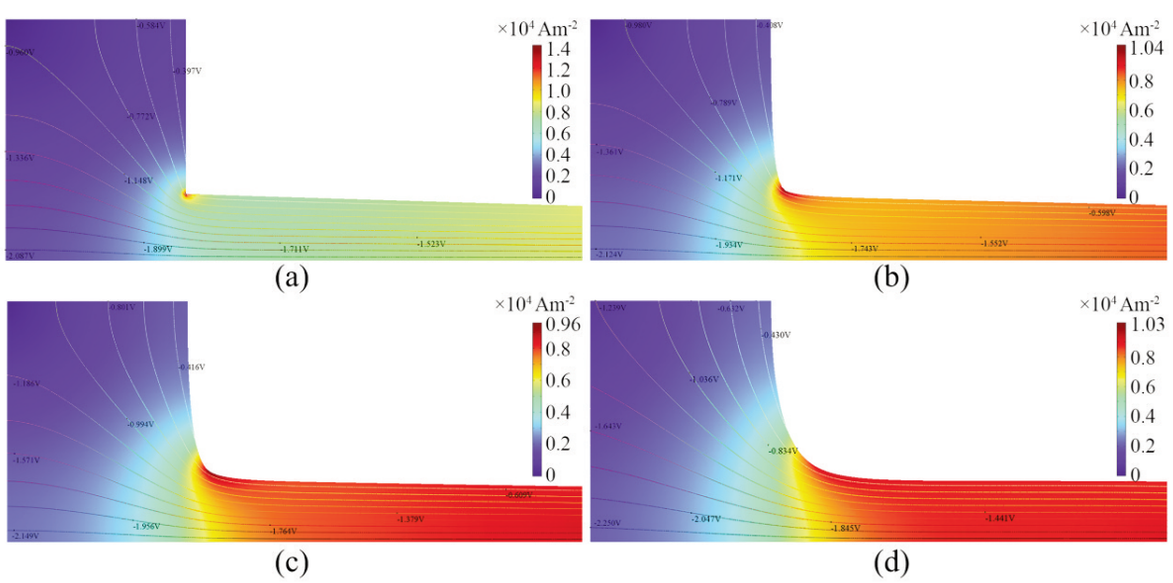

Figure 10. *The anode shapes and secondary current distributions for the anode with a sloped bottom (the tilted angle of 1.7 degrees) at (a) the initial time, after (b) 1 day, (c) 2 days and (d) 5.5 days.*

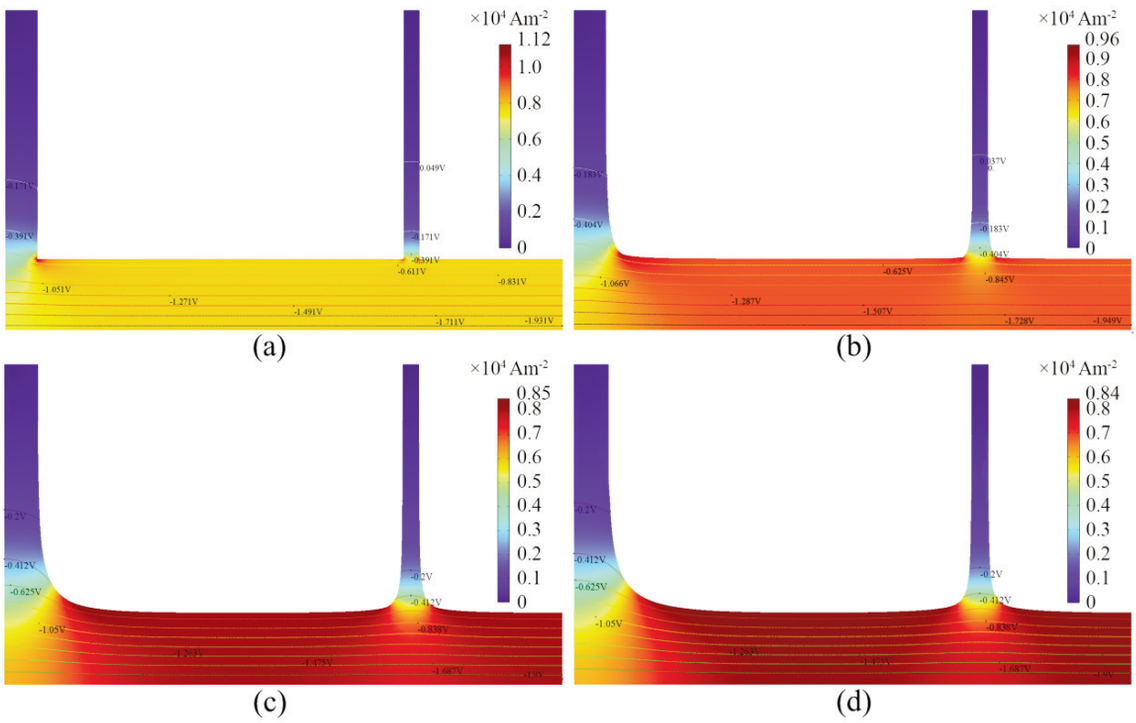

Figure 12. *The anode shapes and secondary current distributions for the anode with slots (1cm width) at (a) the initial time, after (b) 1 day, (c) 4 days and (d) 7 days.*

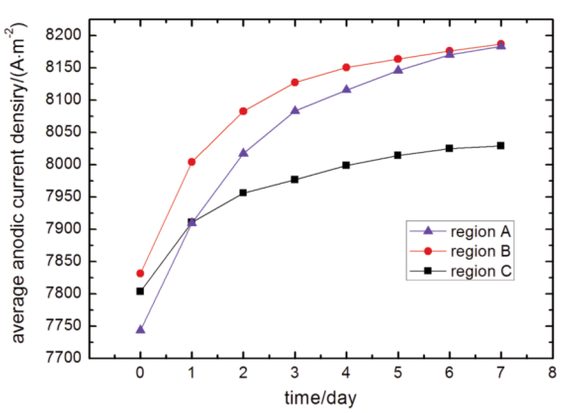

Figure 13. *The changes of the average anodic current densities with respect to time in the different regions of the undersides of the anodes.*

4. Conclusions

The transient calculations for the transformations of the anode shape and the secondary current distribution during electrolysis in aluminium reduction cells were implemented in this study. The results show that the width of the channel and the initial shape of the prebaked anode have important effect on the distribution of anodic current density and the process of anode shape change. It takes more time until the steady state shape is obtained for the anode adjacent to the wider channel, and the fraction of the current passing through the side of the anode increases with the enlargement of the channel width. Cutting off the lower corners of the anode by 4 cm (diagonally) can reduce the time from the initial shape to the constant shape of the anode by 1 day, and making a sloped bottom with the tilted angle of 1.7 degrees can reduce this time by 2.5 days, while, forming two slots in the bottom surface doesn't change this time. The presence of the slots, reducing the area of the working face, increases the anodic current density at the underside of the anode, but leads to the enlargement of the current at the side of the anode to some degree.

Acknowledgement

The authors are grateful for the financial support of the National Natural Science Foundation of China (51274241) and the Foundation for Innovative Research Groups of the National Natural Science Foundation of China (61321003).

References

[1] P. A. Solli, T. Haarberg, T. Eggen, E. Skybakmoen, A. Sterten, Light Metals 1994, ed. U. Mannweiler, The Minerals, Metals and Materials Society, Warrendale, PA, USA, 1994, p.195.

[2] R. Odegard, A. Solheim, K. Thovsen, Light Metals 1992, ed. E. R. Cutschall, The Minerals, Metals and Materials Society, Warrendale, PA, USA, 1992, p.457.

[3] K. J. Fraser, D. Billinghurst, K. L. Chen, J. T. Keniry, Light Metals 1989, ed. P. G. Campbell, The Minerals, Metals and Materials Society, Warrendale, PA, USA, 1989, p.219.

[4] A. Piotrowski, S. Pietrzyk, Metall. & Foundry Eng., 16 (1990) 315-337.

[5] H. Fortin, N. Kandev, M. Fafard, Finite Elem. Anal. Des., 52 (2012) 71-82.

[6] J. Zoric, I. Rousar, J. Thonstad, Z. Kuang, J. Appl. Electrochem., 26(8) (1996) 795-802.

[7] W. W. Hyland, Light Metals 1984, ed. J. P. McGeer, Metallurgical Soc of AIME, Warrendale, PA, USA, 1984, p.711.

[8] D. P. Ziegler, Light Metals 1991, ed. E. Rooy, The Minerals, Metals and Materials Society, Warrendale, PA, USA, 1991, p.363.

[9] J. Zoric, I. Rousar, J. Thonstad, J. Appl. Electrochem., 27(8) (1997) 916-927.

[10] J. Zoric, I. Rousar, J. Thonstad, T. Haarberg, J. Appl. Electrochem., 27(8) (1997) 928-938.

[11] J. Zoric, J. Thonstad, T. Haarberg, Metall. Mater. Trans. B, 30(2) (1999) 341-348.

[12] D. K. Ai. Light Metals 1985, ed. H. O. Bohner, Metallurgical Soc of AIME, Warrendale, PA, USA, 1985, p.607.

[13] G. Franca, C. Mesquita, L. Edwards, F. Vogt, Light Metals 2003, ed. P. N. Crepeau, The Minerals, Metals and Materials Society, Warrendale, PA, USA, 2003, p.535.

[14] O. Zikanov, A. Thess, P. A. Davidson, D. P. Ziegler, Metall. Mater. Trans. B, 31(6) (2000) 1541-1550.

[15] J. Thonstad, P Fellner, G. M. Haarberg, J. Hivas, H. Kvande, A. Sterten, Aluminium Electrolysis, 3rd edn, Aluminium-Verlag, Dusseldorf, 2001, p.159.